Inorg. Chem. **2008**, *47*, 11435−11443

Monoanionic {Mn(NO)}^{5} and Dianionic {Mn(NO)}^{6} Thiolatonitrosylmanganese Complexes: $[(NO)Mn(L)_2]^-$ and $[(NO)Mn(L)_2]^{2-}$ (LH_2 = 1,2-Benzenedithiol and Toluene-3,4-dithiol)

Chia-Huei Lin,[†] Chien-Ge Chen,[†] Ming-Li Tsai,[†] Gene-Hsiang Lee,[‡] and Wen-Feng Liaw*,[†]

Department of Chemistry, National Tsing Hua University, Hsinchu 30013, Taiwan, and Instrumentation Center, National Taiwan University, Taipei, Taiwan

Received August 14, 2008

The reaction of $MnBr_2$ and $[PPN]_2[S,S\text{-}C_6H_3\text{-}R]$ (1:2 molar ratio) in THF yielded $[(THF)Mn(S,S\text{-}C_6H_3\text{-}R)_2]^-$ [R = H (**1a**), Me (**1b**); THF = tetrahydrofuran]. Formation of the dimeric $[Mn(S,S\text{-}C_6H_3\text{-}R)_2]_2^{2-}$ [R = H (**2a**), Me (**2b**)] was presumed to compensate for the electron-deficient Mn^{III} core via two thiolate bridges upon dissolution of complexes **1a** and **1b** in CH_2Cl_2. Complex **2a** displays antiferromagnetic coupling interaction between two Mn^{III} centers (J = -52 cm^{-1}), with the effective magnetic moment (μ_{eff}) increasing from 0.85 μ_B at 2.0 K to 4.86 μ_B at 300 K. The dianionic manganese(II) thiolate complexes $[Mn(S,S\text{-}C_6H_3\text{-}R)_2]^{2-}$ [R = H (**3a**), Me (**3b**)] were isolated upon the addition of $[BH_4]^-$ into complexes **1a** and **1b** or complexes **2a** and **2b**, respectively. The anionic mononuclear {Mn(NO)}^{5} thiolatonitrosylmanganese complexes $[(NO)Mn(S,S\text{-}C_6H_3\text{-}R)_2]^-$ [R = H (**4a**), Me (**4b**)] were obtained from the reaction of NO(g) with the anionic complexes **1a** and **1b**, respectively, and the subsequent reduction of complexes **4a** and **4b** yielded the mononuclear {Mn(NO)}^{6} $[(NO)Mn(S,S\text{-}C_6H_3\text{-}R)_2]^{2-}$ [R = H (**5a**), Me (**5b**)]. X-ray structural data, magnetic susceptibility measurement, and magnetic fitting results imply that the electronic structure of complex **4a** is best described as a resonance hybrid of $[(L)(L)Mn^{III}(NO^{\bullet})]^-$ and $[(L)(L^{\bullet})Mn^{III}(NO^-)]^-$ (L = 1,2-benzenedithiolate) electronic arrangements in a square-pyramidal ligand field. The lower IR ν_{NO} stretching frequency of complex **5a**, compared to that of complex **4a** (shifting from 1729 cm^{-1} in **4a** to 1651 cm^{-1} in **5a**), supports that one-electron reduction occurs in the $\{(L)(L^{\bullet})Mn^{III}\}$ core upon reduction of complex **4a**.

Introduction

Transition-metal nitrosyl complexes have attracted considerable interest stimulated by (i) the versatile bonding properties between metal and NO;[1] (ii) the elucidation of the electronic structure of transition-metal nitrosyls having intrigued inorganic chemists;[2] (iii) the metal nitrosyl complexes being employed to serve as a nitric oxide delivery reagent to biological targets;[3] (iv) the ability of certain transition-metal complexes promoting NO disproportionation to form N_2O and metal nitrite via a metal nitrosyl intermediate;[4] and (v) interactions of NO and heme/nonheme proteins resulting in physiologically relevant M−NO bonds.[5]

Because of the "noninnocent" character of both NO (acting as NO^+, NO^-, and a $NO^{\bullet}$ radical)[6] and a 1,2-benzenedithiolate ligand,[7−11] the determination of formal oxidation states of a transition metal and NO in the 1,2-benzenedithiolatometal nitrosyl complexes may rely on an understanding of what low-lying excited states are present and how this

* To whom correspondence should be addressed. E-mail: wfliaw@mx.nthu.edu.tw.
[†] National Tsing Hua University.
[‡] National Taiwan University.

(1) (a) Ford, P. C.; Bourassa, J.; Lee, K. B.; Lorkovic, I.; Boggs, S.; Kudo, S.; Laverman, L. *Coord. Chem. Rev.* **1998**, *171*, 185. (b) Ford, P. C.; Lorkovic, I. M. *Chem. Rev.* **2002**, *102*, 993. (c) Butler, A. R.; Megson, I. L. *Chem. Rev.* **2002**, *102*, 1155.
(2) (a) Hayton, T. W.; Legzdins, P.; Sharp, W. B. *Chem. Rev.* **2002**, *102*, 935. (b) Hsu, I.-J.; Hsieh, C.-H.; Ke, S.-C.; Chiang, K.-A.; Lee, J.-M.; Chen, J.-M.; Jang, L.-Y.; Lee, G.-H.; Wang, Y.; Liaw, W.-F. *J. Am. Chem. Soc.* **2007**, *129*, 1151.
(3) (a) Cheng, L.; Richter-Addo, G. B. Binding and Activation of Nitric Oxide by Metalloporphyrins and Heme. In *The Porphyrin Handbook*; Guilard, R., Smith, L., Kadish, K. M., Eds.; Academic Press: New York, 2000; Vol. *4*, Chapter 33. (b) Afshar, R. K.; Patra, A. K.; Mascharak, P. K. *J. Inorg. Biochem.* **2005**, *99*, 1458.
(4) Averill, B. A. *Chem. Rev.* **1996**, *96*, 2951.
(5) Richter-Addo, G. B.; Legzdins, P. *Metal Nitrosyls*; Oxford University: New York, 1992.
(6) (a) Pierpont, C. G.; Buchanan, R. M. *Coord. Chem. Rev.* **1981**, *38*, 45. (b) Attia, A. S.; Pierpont, C. G. *Inorg. Chem.* **1995**, *34*, 1172. (c) Wang, P. G.; Xian, M.; Tang, X.; Wu, X.; Wen, Z.; Cai, T.; Janczuk, A. J. *Chem. Rev.* **2002**, *102*, 1091.

10.1021/ic801553s CCC: $40.75
Published on Web 11/07/2008

Scheme 1

$$[(L)(L)\text{-}Mn^{II}\text{-}(NO^{+})]^{-} \leftrightarrow [(L)(L)\text{-}Mn^{III}\text{-}(NO^{\bullet})]^{-} \leftrightarrow [(L^{\bullet})(L)\text{-}Mn^{III}\text{-}(NO^{-})]^{-}$$

A (unpaired NO electron in Mn orbital) **B** (unpaired NO electron in NO itself) **C** (unpaired NO electron as well as the electron from one of the L^{2-} in NO)

affects the electronic spectroscopy,[11] although the metal−NO unit has so far been generally designated by $\{M(NO)_x\}^n$, where n = total number of electrons in the valence orbitals of the metal ion and π^* orbitals of NO, known as Enemark−Feltham notation.[8,12] Recently, some interesting compounds of NO binding metal centers such as $M-NO^+$/$M-NO^-$/$M-NO^{\bullet}$ have been reported.[9−11] Though Fe−N−O is almost linear [Fe−N−O = 174.3(4)°] and the Fe−N bond length is as low as 1.670(4) Å, Lippard and co-workers[7] concluded on the basis of electron paramagnetic resonance (EPR), Mössbauer spectroscopy, SQUID susceptometry, and normal-coordinate analysis that the structure of [(NO)Fe(TC-5,5)] (TC-5,5 = tropocoronand) is a trigonal bipyramid with a low-spin-state $\{Fe^{III}(NO^-)\}$ electronic structure.[9] On the basis of Mössbauer spectroscopy and EPR measurements, Wieghardt and co-workers concluded that the electronic structure of $[Fe(H_2O)_5(NO)]^{2+}$ is best described as $[Fe^{III}(H_2O)_5(NO^-)]^{2+}$ with Fe^{III} antiferromagnetically coupled to NO^- ($S = 1$), yielding the observed spin quartet ground state ($S = {}^3/_2$).[10] Interestingly, the experimental and theoretical studies conducted by Wanner et al. show that $[(NC)_5Fe(NO)]^{3-}$ contains delocalized oxidation levels of the metal and ligand, namely, a resonance hybrid of $[(NC)_5Fe^{II}(NO^{\bullet})]^{3-}$ and $[(NC)_5Fe^{I}(NO^{+})]^{3-}$.[11]

In spite of a large number of mononuclear $\{Mn(NO)\}^6$ and $\{Mn(NO)\}^7$ manganese nitrosyl complexes known,[2b,13] no examples of mononuclear $\{Mn(NO)\}^5$ thiolatonitrosylmanganese complexes are reported. The present investigation was therefore initiated to uncover the electronic structure and reactivity of the unexplored $\{Mn(NO)\}^5$ thiolatonitrosylmanganese complexes by introducing the redox-active 1,2-benzenedithiolate serving as good σ- and π-donating coligands. By application of nitrosylation of $[(THF)Mn(S,S\text{-}C_6H_3\text{-}R)_2]^-$ [R = H (**1a**), Me (**1b**); THF = tetrahydrofuran], the anionic $\{Mn(NO)\}^5$ $[(NO)Mn(S,S\text{-}C_6H_3\text{-}R)_2]^-$ [R = H (**4a**), Me (**4b**)] complexes were prepared. Because of the noninnocent nature of the ligands, three resonate forms of $\{Mn(NO)\}^5$ $[(NO)Mn(S,S\text{-}C_6H_3\text{-}R)_2]^-$ can be described as in Scheme 1. The dianionic, mononuclear $\{Mn(NO)\}^6$ $[(NO)Mn(S,S\text{-}C_6H_3\text{-}R)_2]^{2-}$ [R = H (**5a**), Me (**5b**)] complexes were produced upon the reduction of complexes **4a** and **4b** by $[S,NH_2\text{-}C_6H_4]^-$, respectively. Oxygen oxidation of the $\{Mn(NO)\}^6$ complexes **5a** and **5b** leads to the formation of complexes **4a** and **4b** and the major product $[Mn(S,S\text{-}C_6H_3\text{-}R)_3]^{2-}$ [R = H (**6a**), Me (**6b**)], respectively.[15]

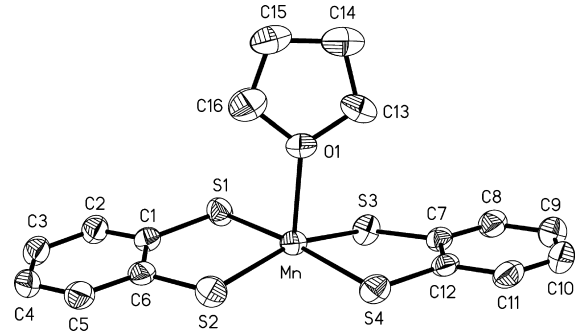

Figure 1. ORTEP drawing of the anionic part ($[(THF)Mn(S,S\text{-}C_6H_4)_2]^-$) of complex **1a** with thermal ellipsoids drawn at the 50% probability level. Selected bond distances (Å) and angles (deg): Mn−O1 2.250(3), Mn−S1 2.3035(12), Mn−S2 2.3052(12), Mn−S3 2.2954(12), Mn−S4 2.3092(12); O1−Mn−S3 99.07(9), S3−Mn−S1 87.57(4), S3−Mn−S2 158.91(5), O1−Mn−S4 93.92(8), S1−Mn−S4 171.17(5), O1−Mn−S2 101.94(9), O1−Mn−S1 94.43(8).

Results and Discussion

Synthetic and Characterization Aspects: Interconversion among $[(THF)Mn(L)_2]^-$, $[Mn(L)_2]_2^{2-}$, and $[Mn(L)_2]^{2-}$ (THF = tetrahydrofuran; L = 1,2-Benzenedithiolate and Toluene-3,4-dithiolate). The anionic mononuclear manganese thiolate complexes $[(THF)Mn(S,S\text{-}C_6H_3\text{-}R)_2]^-$ [R = H (**1a**), Me (**1b**); THF = tetrahydrofuran] containing $[S,S\text{-}C_6H_3\text{-}R]^{2-}$ and $[C_4H_8O]$ ligands bound to manganese in a bidentate and a monodentate manner, respectively, were obtained when a MeOH solution of 2 equiv of $[Na]_2[S,S\text{-}C_6H_3\text{-}R]$ and $MnBr_2$ was added to a THF solution of [PPN][Cl] (or $[Et_4N][Br]$). Presumably, the role of a THF ligand coordinated to a Mn^{III} center in complex **1a** is to compensate for the electron deficiency of the Mn^{III} center as well as to stabilize the Mn^{III}

(7) (a) Franz, K. J.; Lippard, S. J. *J. Am. Chem. Soc.* **1998**, *120*, 9034. (b) Brown, C. A.; Pavlosky, M. A.; Westre, T. E.; Zhang, Y.; Hedman, B.; Hodgson, K. O.; Solomon, E. I. *J. Am. Chem. Soc.* **1995**, *117*, 715. (c) Mingos, D. M. P.; Sherman, D. J. *Adv. Inorg. Chem.* **1989**, *34*, 293.
(8) Enemark, J. H.; Feltham, R. D. *Coord. Chem. Rev.* **1974**, *13*, 339.
(9) Franz, K. J.; Lippard, S. J. *J. Am. Chem. Soc.* **1999**, *121*, 10504.
(10) (a) Wanat, A.; Schneppensieper, T.; Stochel, G.; van Eldik, R.; Bill, E.; Wieghardt, K. *Inorg. Chem.* **2002**, *41*, 4. (b) Ray, K.; Weyhermüller, T.; Goossens, A.; Crajé, M. W. J.; Wieghardt, K. *Inorg. Chem.* **2003**, *42*, 4082. (c) Ghosh, P.; Stobie, K.; Bill, E.; Bothe, E.; Weyhermüller, T.; Ward, M. D.; McCleverty, J. A.; Wieghardt, K. *Inorg. Chem.* **2007**, *46*, 522. (d) Herebian, D.; Bothe, E.; Bill, E.; Weyhermuller, T.; Wieghardt, K. *J. Am. Chem. Soc.* **2001**, *123*, 10012. (e) Chaudhuri, P.; Verani, C. N.; Bill, E.; Bothe, E.; Weyhermuller, T.; Wieghardt, K. *J. Am. Chem. Soc.* **2001**, *123*, 2213.
(11) Wanner, M.; Scheiring, T.; Kaim, W.; Slep, L. D.; Baraldo, L. M.; Olabe, J. A.; Zalis, S.; Baerends, E. J. *Inorg. Chem.* **2001**, *40*, 5704.
(12) (a) Enemark, J. H.; Feltham, R. D. *Proc. Natl. Acad. Sci. U.S.A.* **1972**, *69*, 3534. (b) Leverman, L. E.; Wanat, A.; Oszajca, J.; Stochel, G.; Ford, P. C.; van Eldik, R. *J. Am. Chem. Soc.* **2001**, *123*, 285. (c) Gray, H. B.; Bernal, I.; Billig, E. *J. Am. Chem. Soc.* **1962**, *84*, 3404.
(13) (a) Scheidt, W. R.; Hatano, K.; Rupprecht, G. A.; Piciulo, P. L. *Inorg. Chem.* **1979**, *18*, 292. (b) Ghosh, K.; Eroy-Reveles, A. A.; Avila, B.; Holman, T. R.; Olmstead, M. M.; Mascharak, P. K. *Inorg. Chem.* **2004**, *43*, 2988. (c) Zahran, Z. N.; Shaw, M. J.; Khan, M. A.; Richter-Addo, G. B. *Inorg. Chem.* **2006**, *45*, 2661.
(14) Greiwe, K.; Krebs, B.; Henkel, G. *Inorg. Chem.* **1989**, *28*, 3713.
(15) (a) Lee, C.-M.; Hsieh, C.-H.; Dutta, A.; Lee, G.-H.; Liaw, W.-F. *J. Am. Chem. Soc.* **2003**, *125*, 11492. (b) Lee, C.-M.; Chen, C.-H.; Chen, H.-W.; Hsu, J.-L.; Lee, G.-H.; Liaw, W.-F. *Inorg. Chem.* **2005**, *44*, 6670.
(16) Hsieh, C.-H.; Hsu, I.-J.; Lee, C.-M.; Ke, S.-C.; Wang, T.-Y.; Lee, G.-H.; Wang, Y.; Chen, J.-M.; Lee, J.-F.; Liaw, W.-F. *Inorg. Chem.* **2003**, *42*, 3925.

Scheme 2

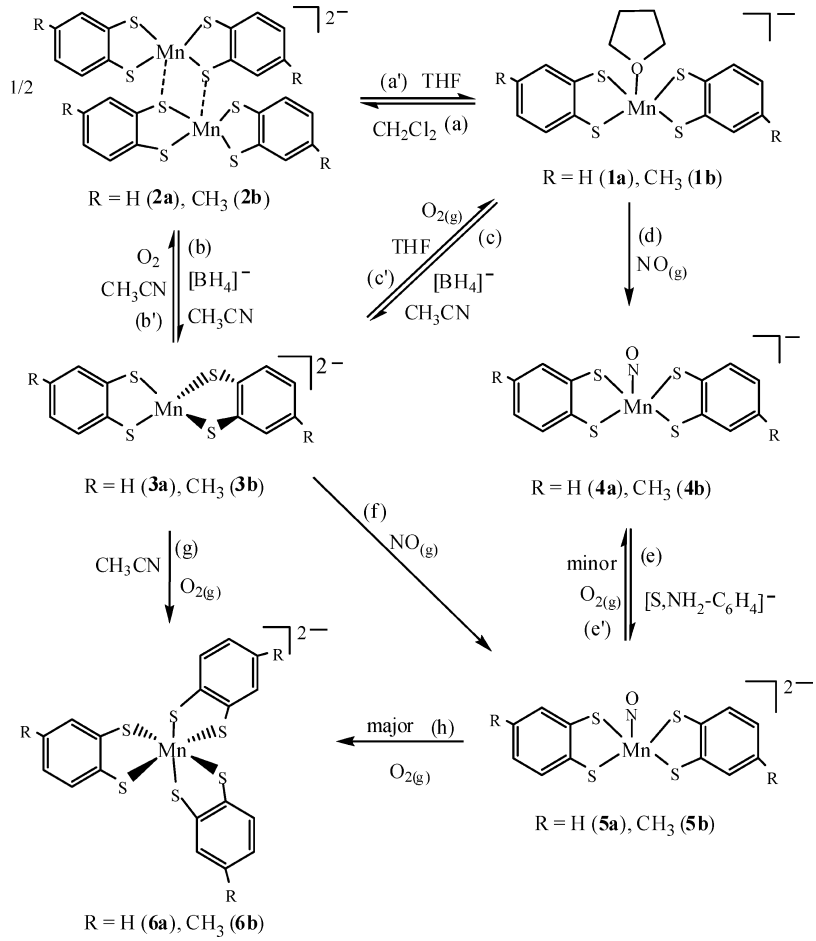

oxidation level. The ^{1}H NMR spectrum of complex **1a** at 298 K exhibits the paramagnetic shifts that appear at δ −8.16 (br), −22.95 (br) (S,S-C_6H_4), 3.62 (s), 1.78 (s) (C_4H_8O) ppm (C_4D_8O). The temperature-independent effective magnetic moment (μ_B) in the solid state by a SQUID magnetometer was 4.84 μ_B for complex **1a** (Figure S1 in the Supporting Information), consistent with a total spin value (S_T) of 2.

In contrast to the formation of the mononuclear, distorted square-pyramidal complexes **1a** and **1b** in THF, the formation of the stable dimeric $[Mn(S,S\text{-}C_6H_3\text{-}R)_2]_2^{2-}$ [R = H (**2a**), Me (**2b**)] was observed when complexes **1a** and **1b** were dissolved in CH_2Cl_2, respectively (Scheme 2a). Coordinative association of two anionic mononuclear $[Mn(S,S\text{-}C_6H_3\text{-}R)_2]^-$ complexes yielding complexes **2a** and **2b** in the absence of a THF-coordinating solvent, respectively, is attributed to the avoidance of electron deficiency at the Mn^{III} centers as well as to the availability of the nonbonding electron pairs of the sulfur atoms in the $[Mn(S,S\text{-}C_6H_3\text{-}R)_2]^-$ complex. In contrast to the temperature-independent effective magnetic moment observed in **1a**, **2a** shows that its μ_{eff} decreases from 4.68 μ_B at 300 K to 0.85 μ_B at 2.0 K (Figure S2 in the Supporting Information) and **2b** shows a decrease from 4.80 μ_B at 300 K to 0.64 μ_B, with 0.5 T applied field in both cases (Figure S3a in the Supporting Information). Thus, the electronic structures of complexes **2a** and **2b** can be best described as two paramagnetic d^4 Mn^{III} cores with antiferromagnetic coupling ($J = -52$ cm^{-1}) with TIP held constant at 200 × 10^{-6} cm^3 mol^{-1} for **2b** (Figure S3b in the Supporting Information), i.e., both centers having $S = 2$ spins magnetically couple to each other possibly via the direct metal d−d orbital overlap (Mn1···Mn1A = 3.365 Å) and the bridging sulfurs [Mn1···S4 = 2.594(1) Å for **2b**].

As presented in Scheme 2b, upon the addition of $[BH_4]^-$ into CH_3CN of complexes **2a** and **2b** in a 2:1 stoichiometry under nitrogen at room temperature, respectively, a reaction ensued over the course of 3 h to yield the dianionic mononuclear manganese thiolate complexes $[Mn(S,S\text{-}C_6H_3\text{-}R)_2]^{2-}$ [R = H (**3a**), Me (**3b**)].[14] Also, the temperature-independent effective magnetic moment in the solid state by a SQUID magnetometer was 6.15 μ_B for complex **3a**, which is consistent with the Mn^{II} ion having a high-spin d^5 electronic configuration in a tetrahedral ligand field.[15] Alternatively, treatment of complex **1a** with 1 equiv of $[BH_4]^-$ in CH_3CN for 1 h at ambient temperature also led to the reduction of complex **1a** to produce complex **3a** (Scheme 2c). Consistent with complex $[(THF)Fe(S,S\text{-}C_6H_4)_2]^-$,[15] complex **3a** does not initiate O_2 activation to yield manganese sulfinate/sulfenate compounds identified by IR ν_{SO}. Instead, purging of a THF solution of complex **3a** by O_2 yielded complex **1a** (Scheme 2c′).

Structures of Complexes 1a, 2b, and 3a. Figures 1−3 display the thermal ellipsoid plots of complexes **1a**, **2b**, and **3a**, respectively, and selected bond distances and angles are given in the figure captions. The O1−Mn−S3, O1−Mn−S4,

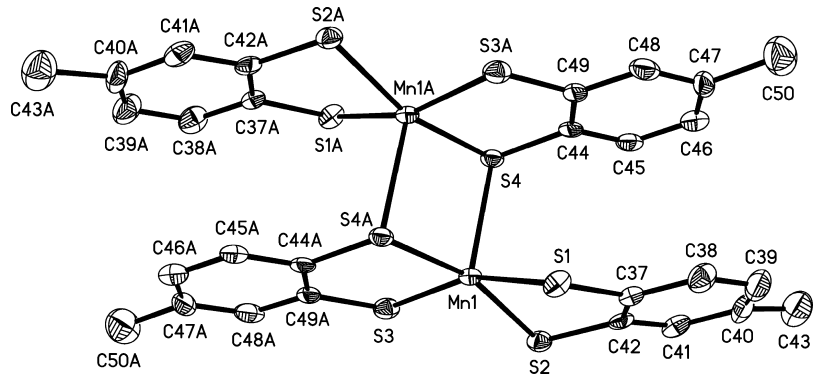

Figure 2. ORTEP drawing of the anionic part ($[Mn(S,S\text{-}C_6H_3\text{-}Me)_2]_2^{2-}$) of complex **2b** with thermal ellipsoids drawn at the 50% probability level. Selected bond distances (Å) and angles (deg): Mn1−S3 2.2933(9), Mn1−S1 2.2978(9), Mn1−S2 2.999(9), Mn1−S4A 2.3411(9), Mn1···S4 2.5938(10), Mn1···Mn1A 3.365; S3−Mn1−S1 159.33(4), S3−Mn1−S2 86.09(3), S1−Mn1−S2 87.85(3), S3−Mn1−S4A 88.47(3).

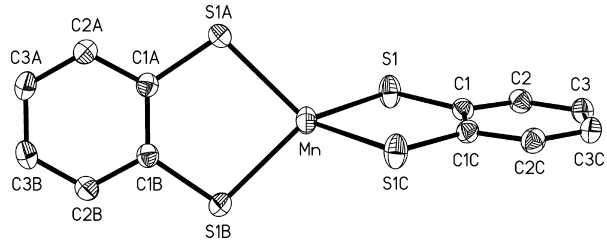

Figure 3. ORTEP drawing of the anionic part ($[Mn(S,S\text{-}C_6H_4)_2]^{2-}$) of complex **3a** with thermal ellipsoids drawn at the 50% probability level. Selected bond distances (Å) and angles (deg): Mn−S1A 2.4230(5), Mn−S1B 2.4230(5), Mn−S1 2.4230(5), Mn−S1C 2.4230(5); S1−Mn−S1C 88.50(2), S1C−Mn−S1A 131.68(3), S1−Mn−S1A 111.18(3), S1C−Mn−S1B 111.18(3), S1−Mn−S1B 131.68(3), S1B−Mn−S1A 88.50(2).

S3−Mn−S1, and S1−Mn−S4 bond angles of 99.07(9), 93.92(8), 87.57(4), and 171.17(5)°, respectively, are consistent with the distorted square-pyramidal coordination environment about manganese of complex **1a**. The displaced distance (0.2942 Å) of the manganese atom from the mean four-sulfur-atom plane toward the axial THF was observed in complex **1a**. The dinuclear complex **2b** is electronically dianionic, and therefore both manganese atoms should be Mn^{III}. Complex **2b** possesses crystallographically imposed centrosymmetry. Two $[Mn(S,S\text{-}C_6H_3CH_3)_2]^-$ units are connected via two thiolate bridges [Mn1···S4 = 2.594(1) Å] in complex **2b**. It is noticed that the average Mn−S bond lengths of 2.3033(12) and 2.3080(9) Å in complexes **1a** and **2b**, respectively, are shorter than that of 2.4230(5) Å in complex **3a** (Table S1 in the Supporting Information). The reduction of complex **1a** to **3a** (Mn^{III} to Mn^{II}) was believed to cause the elongation of the mean Mn−S bond distances. The geometry of the manganese center of complex **3a** is best described as a distorted tetrahedral with S1−Mn−S1A, S1−Mn−S1B, S1−Mn−S1C, and S1A−Mn−S1C bond angles of 111.18(3), 131.68(3), 88.50(2), and 131.68(3)°, respectively.

Syntheses of the Anionic $\{Mn(NO)\}^5$ $[(NO)Mn(S,S\text{-}C_6H_3\text{-}R)_2]^-$ and Dianionic $\{Mn(NO)\}^6$ $[(NO)Mn(S,S\text{-}C_6H_3\text{-}R)_2]^{2-}$ (R = H, CH_3). Upon bubbling of NO(g) (10% NO + 90% N_2) through THF solutions of complexes **1a** and **1b**, respectively, IR [ν_{NO}: 1735 s (THF), 1727 s (KBr) cm^{-1} (**4a**)] and UV−vis spectra implied the formation of the anionic $\{Mn(NO)\}^5$ complex $[(NO)Mn(S,S\text{-}C_6H_3\text{-}R)_2]^-$ [R = H (**4a**), Me (**4b**); Scheme 2d]. Complex **4a** was isolated and

Scheme 3

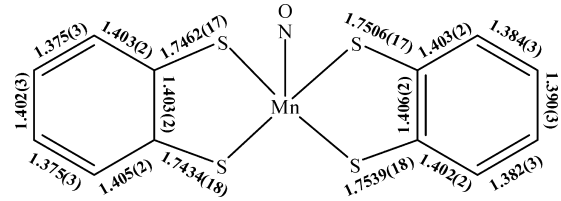

(4a)

characterized by single-crystal X-ray analysis. Upon bubbling of nitrogen into a THF solution of complex **4a**, the identical IR ν_{NO} stretching frequency and UV−vis absorption bands demonstrated that complex **4a** is stable under a nitrogen atmosphere. In order to elucidate the valence state distribution pattern of the $\{(L)_2Mn(NO)\}^5$ (L = S,S-C_6H_3-R) core, the criteria [the C−S bond distance of 1.735(6) Å and the alternative patterns of two shorter C═C (ave 1.380 Å) as well as four longer C═C bonds (ave 1.406 Å) denoting the radical monoanion $[L^{\bullet}]^-$ electronic state (L = 1,2-benzenedithiolate)] reported by Wieghardt and co-workers were adopted.[6,10] The C−S bond length of 1.745 Å in combination with the alternative patterns of two shorter C═C (ave 1.375 Å) and four longer C═C (ave 1.403 Å) bonds implies the existence of a π-radical monoanionic 1,2-benzenedithiolate in complex **4a**, as shown in Scheme 3. The temperature-dependent effective magnetic moment (μ_{eff}) increases from 3.25 μ_B at 2.0 K to 4.77 μ_B at 300 K (Figure 4). These results imply that the electronic structure of complex **4a** may adopt a resonance hybrid of $[(L)(L)Mn^{III}(NO^{\bullet})]^-$ and $[(L)(L^{\bullet})Mn^{III}(NO^-)]^-$ electronic configurations in a square-pyramidal ligand field.

When THF solutions of complexes **4a** and **4b** were treated with 1 equiv of $[S,NH_2\text{-}C_6H_4]^-$, respectively, instead of the direct nucleophilic attack of $[S,NH_2\text{-}C_6H_4]^-$ on the coordinated NO yielding $[ON\text{-}S,NH_2\text{-}C_6H_4]$ and $[Mn(S,S\text{-}C_6H_3\text{-}R)_2]^{2-}$, UV−vis, IR spectra, and X-ray diffraction studies confirmed the formation of the dianionic, mononuclear $\{Mn(NO)\}^6$ $[(NO)Mn(S,S\text{-}C_6H_3\text{-}R)_2]^{2-}$ [R = H (**5a**), Me (**5b**)] accompanied by byproduct 2-aminophenyl disulfide identified by ^1H NMR (Scheme 2e). The temperature-dependent effective magnetic moment (μ_{eff}) of complex **5a** increases from 2.86 μ_B at 2 K to 3.59 μ_B at 300 K (Figure 5). The most noteworthy characteristic of the reduction of

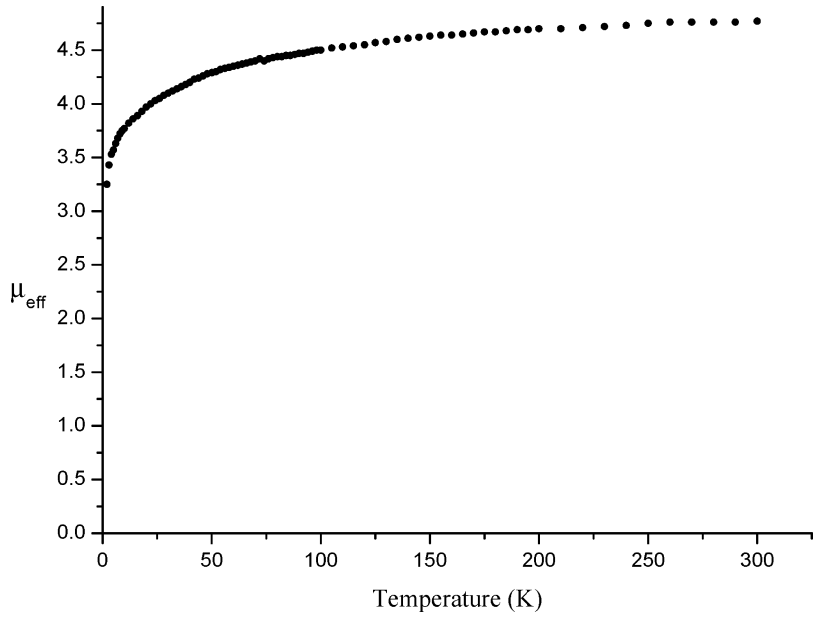

Figure 4. Plot of the effective magnetic moment (μ_B) vs temperature for complex **4a**.

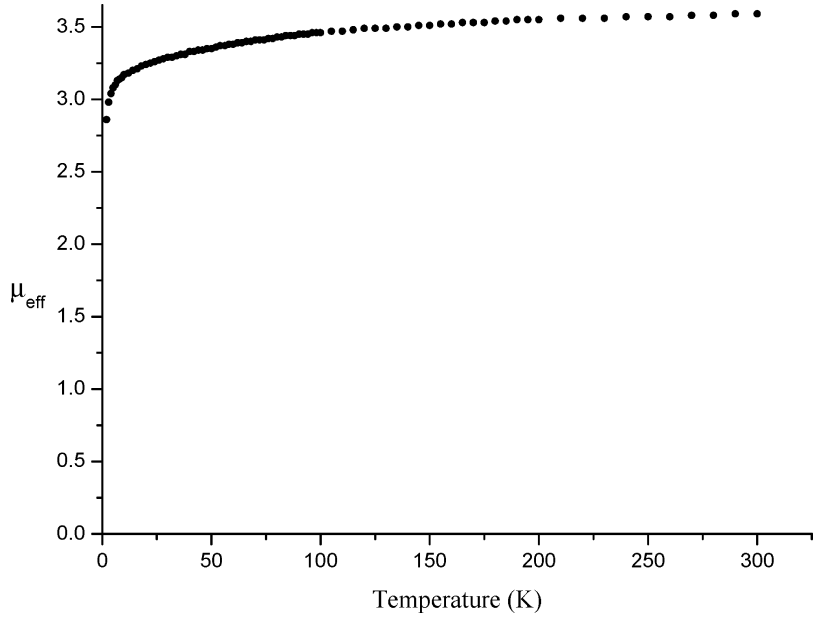

Figure 5. Plot of the effective magnetic moment (μ_B) vs temperature for complex **5a**.

complex **4b** is the disappearance of the low-energy absorption band at 740 nm with concomitant formation of 665 and 357 nm absorption bands. No optical evidence (based on the UV−vis spectrum) for the presence of [S,S-C_6H_3R]$^\bullet$ was observed.[10,15] It is believed that relief of the electron deficiency of the {Mn(NO)} core due to reduction does not require electronic compensation from the "redox-noninnocent" 1,2-benzenedithiolate(2−) ligand. The lower energy ν_{NO} band [1650 cm^{-1} (KBr)] of complex **5b** shifted by 76 cm^{-1} from that of complex **4b** [1727 cm^{-1} (KBr)] implies that the reduction process occurred in the {(L)(L$^\bullet$)Mn^{III}} core. These results indicate that the electronic structure of the {Mn(NO)}^{6} core of complex **5b** may exist as {(L)(L)-$Mn^{III}(NO^-)$}, i.e., the {Mn(NO)}^{6} **5b** having a high-spin d^4 $Mn^{III}NO^-$ electronic configuration in a distorted square-pyramidal ligand field,[9] although the Mn1−N1−O1 bond angle of 176.87(14)° in complex **4a** is comparable to that of 177.2(6)° in complex **5a**. Alternatively, when complex **3a** (or **3b**) was treated with NO(g) (10% NO + 90% N_2) in CH_3CN at room temperature, a rapid reaction ensued over the course of 5 min to give the air-sensitive, deep-green complex **5a** (or **5b**), as shown in Scheme 2f.

Magnetic Susceptibility Study. To further understand the chemical properties of complexes **4a** and **5a**, the detailed description of the electronic structure is imperative, specifically, the oxidation states of manganese and NO. In complex **4a**, four possible electronic structures of {(L)(•L)MnNO} (L = 1,2-benzenedithiolate) with a radical monoanion (•L) serving as a coligand can be depicted; i.e., {(L)(•L)$Mn^{I}NO^+$} ($S_{\bullet L}$ = $^1/_2$, S_{Mn} = 2, S_{NO} = 0), {(L)(•L)Mn^{II}(•NO)} ($S_{\bullet L}$ = $^1/_2$, S_{Mn} = $^5/_2$, S_{NO} = $^1/_2$), {(L)(•L)$Mn^{III}NO^-$} ($S_{\bullet L}$ = $^1/_2$, S_{Mn} = 2, S_{NO} = 1), and

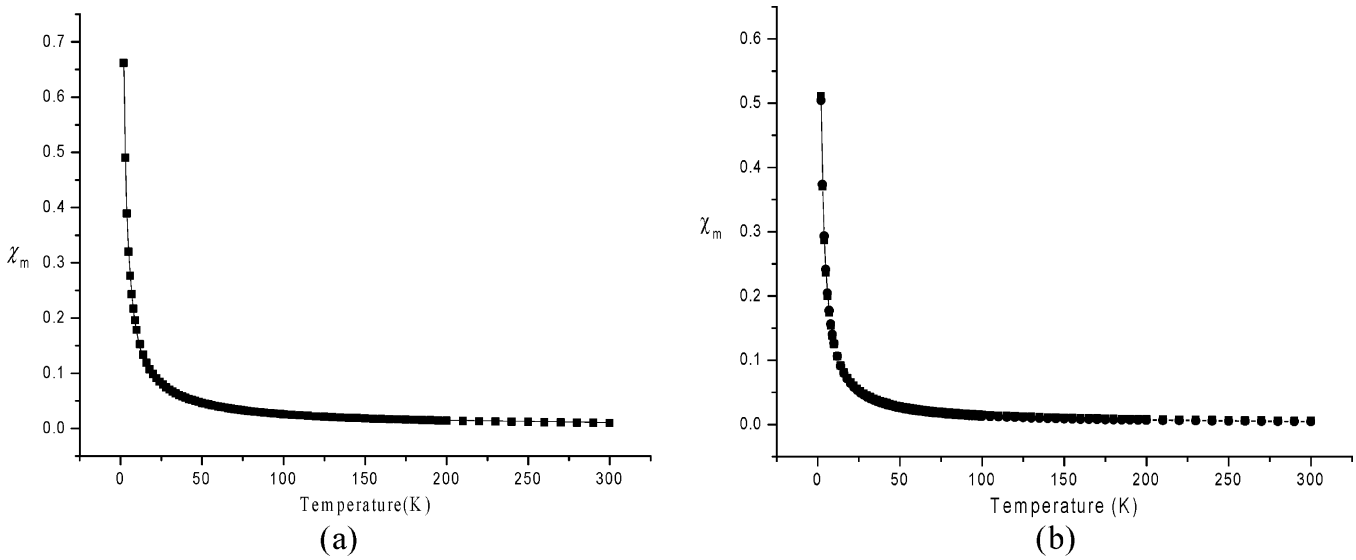

Figure 6. (a) Least-squares fit ($R^2 = 0.982$) to the χ_M vs temperature (2−300 K) curve for complex **4a**, shown as a solid line, giving $J = -25$ cm^{-1}, $\theta = -0.8277$ cm^{-1}, $g = 2$ (fixed), with TIP held constant at 200×10^{-6} cm^3 mol^{-1}. (b) Least-squares fit to the χ_M vs temperature (2−300 K) curve for complex **5a**, shown as a solid line, giving $g = 2$ (fixed), $|D| = 2.05$, and $|E| = 0.0473$. (The values of D and E are shown by their absolute values because the sign cannot be unambiguously determined by fitting of the powder susceptibility data). The results were fitted by using the program *ANISOFIT* (Shores, M. P.; Sokol, J. J.; Long, J. R. *J. Am. Chem. Soc.* **2002**, *124*, 2279−2292; assuming that only the ground state is populated) including axial zero-field splitting (D), rhombicity of the system (E), and Zeeman interactions and incorporate a full powder average.

$\{(L)(^{\bullet}L)Mn^{III}NO^{-}\}$ ($S_{\bullet L} = {}^1/_2$, $S_{Mn} = 2$, $S_{NO} = 0$).[10c] In order to validate the most possible electronic structure of {(L)(•L)MnNO}, a magnetochemical study suitable for elucidating interactions of unpaired electrons in a spin-coupled system was conducted. The spin Hamiltonian of isotropic spin exchange of three-spin and two-spin centers, respectively, can be expressed as

$$\hat{H}_{3spin} = -J_1\hat{S}_{Fe}\cdot\hat{S}_{NO} - J_2\hat{S}_{Fe}\cdot\hat{S}_{L} - J_3\hat{S}_{NO}\cdot\hat{S}_{L} \quad (1)$$

$$\hat{H}_{2spin} = -J\hat{S}_{Fe}\cdot\hat{S}_{L} \quad (2)$$

Several attempts have been made to fit the magnetic susceptibility data of complex **4a** based on the electronic structures described above. Results show that the electronic structure of $\{(L)(^{\bullet}L)Mn^{III}NO^{-}\}$ ($S_{\bullet L} = {}^1/_2$, $S_{Mn} = 2$, $S_{NO} = 0$) fits the experimental susceptibility data (Figure 6a) because the detailed comparisons of the average Mn−S bond distances rule out the possibility of a $\{(L)(^{\bullet}L)Mn^{I}NO^{+}\}$ electronic structure (Tables S1 and S2 in the Supporting Information). The analytical expression of χ_m is given below (χ_m is the molar susceptibility, J is the exchange coupling parameter, TIP is temperature-independent paramagnetism, and θ is a Weiss-like temperature correction; all other terms have their usual significances).

$$\hat{H}_{3spin} = -J_1\hat{S}_{Fe}\cdot\hat{S}_{NO} - J_2\hat{S}_{Fe}\cdot\hat{S}_{L} - J_3\hat{S}_{NO}\cdot\hat{S}_{L} \quad (3)$$

The magnetic behavior of complex **5a** can also be fitted properly by $\{(L)(L)Mn^{III}NO^{-}\}$ ($S_L = 0$, $S_{Mn} = 2$, and $S_{NO} = 0$; Figure 6b) modeled by spin Hamiltonian (4).

$$\hat{H} = D\hat{S}_z^{\,2} + E(\hat{S}_x^{\,2} + \hat{S}_y^{\,2}) + g_{iso}\mu_B B\cdot S \quad (4)$$

On the basis of the magnetochemical studies in combination with average Mn−S bond lengths of 2.2637(5) Å for complex **4a** and 2.259(1−2) Å for complex **5a**, the electronic structure of complex **4a** may be best described as a resonance hybrid of $[(L)(L)Mn^{III}(NO^{\bullet})]^{-}$ and $[(L)(L^{\bullet})Mn^{III}(NO^{-})]^{-}$ ($S_{\bullet L} = {}^1/_2$, $S_{Mn} = 2$, $S_{NO} = 0$) with intramolecular antiferromagnetic coupling between manganese and radical monoanion (•L)/nitric oxide (NO•), respectively. Also, because of the low-energy absorption band (740 nm) tentatively assigned as the existence of $[S,S\text{-}C_6H_3R]^{\bullet}$,[10] we cannot rule out the existence of the $[(L)(L^{\bullet})Mn^{III}(NO^{-})]^{-}$ resonance form in complex **4a**. Complex **5a** is best characterized as a $\{(L)(L\text{-})Mn^{III}NO^{-}\}$ ($S_L = 0$, $S_{Mn} = 2$, $S_{NO} = 0$) electronic structure possessing tetragonal distortion imposed by an axial NO^{-} ligand, consistent with the previous assignments.

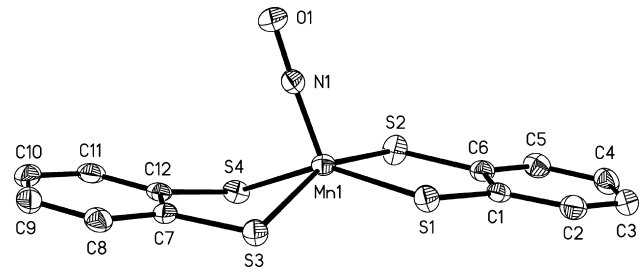

Figure 7. ORTEP drawing of the anionic part ($[(NO)Mn(S,S\text{-}C_6H_4)_2]^{-}$) of complex **4a** with thermal ellipsoids drawn at the 50% probability level. Selected bond distances (Å) and angles (deg): Mn1−N1 1.6355(14), Mn1−S1 2.2579(5), Mn1−S2 2.2474(5), Mn1−S3 2.2793(5), Mn1−S4 2.2703 (5), N1−O1 1.1861(18); S3−Mn1−N1 99.56(5), S3−Mn1−S4 86.906(17), S2−Mn1−S1 87.882(18), S2−Mn1−S4 86.691(18), S1−Mn1−S4 150.220(19), S1−Mn1−S3 86.049(17), S3−Mn1−S2 155.55(2), S2−Mn1−N1 104.55(5), S1−Mn1−N1 113.95(5), S4−Mn1−N1 95.75(5), O1−N1−Mn1 176.87(14).

Structures of Complexes 4a and 5a. X-ray crystal structures of complexes **4a** and **5a** are depicted in Figures 7 and 8, respectively, and selected bond dimensions for both complexes are presented in the figure captions. Analysis of the bond angles for complex **4a** reveals that the coordination geometry of the manganese center is best described as a distorted square pyramid with a linear apical NO and a dihedral angle of 38° (between planes S1−Mn1−S2 and

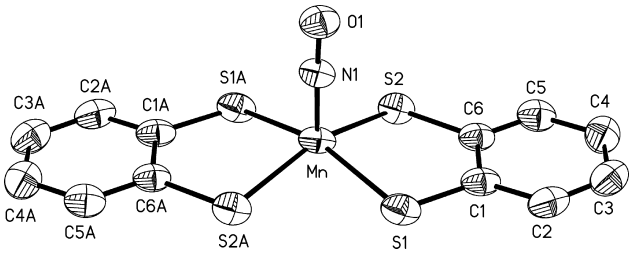

Figure 8. ORTEP drawing of the anionic part ($[(NO)Mn(S,S\text{-}C_6H_4)_2]^{2-}$) of complex **5a** with thermal ellipsoids drawn at the 50% probability level. Selected bond distances (Å) and angles (deg): Mn1−N1 1.607(6), Mn1−S1A 2.2966(14), Mn1−S2 2.2753(16), Mn1−S2A 2.2380(15), Mn1−S1 2.2249(15), N1−O1 1.206(8); Mn1−N1−O1 177.2(6), S1A−Mn1−N1 101.9(2), S1−Mn1−N1 100.8(2), S2A−Mn1−N1 100.3(2), S1A−Mn1−S1 157.29(5), S2−Mn1−N1 102.4(2), S1A−Mn1−S2 86.57(5), S1A−Mn1−S2A 87.23(5), S2−Mn1−S2A 157.19(5), S2−Mn1−S1 88.07(6).

S3−Mn1−S4). The manganese atom is displaced from the mean four-sulfur-atom plane (0.5304 Å for **4a**). Compared to the Mn−N(O) and N−O bond lengths of 1.6355(14) and 1.1861(18) Å, respectively, for $\{Mn(NO)\}^5$ complex **4a**, relief of the electron deficiency from reduction may explain the observed shortening and lengthening of the Mn−N(O) and N−O bond lengths [1.607(6) and 1.206(8) Å, respectively] for $\{Mn(NO)\}^6$ complex **5a** (Table S2 in the Supporting Information). However, the average Mn−S bond lengths are not affected by the electronic change going from $\{Mn(NO)\}^5$ to $\{Mn(NO)\}^6$ [2.2637(5) Å for complex **4a** vs 2.259(1−2) Å for complex **5a**]. It is also noticed that the N−O bond length of 1.206(8) Å in complex **5a**, longer than that of 1.186(18) Å in complex **4a**, is nearly midway between the N−O bond distance of 1.154 Å in free •NO and 1.26 Å in NO^-. Consistent with the previous discussion, the electronic structure of the $\{Mn(NO)\}^6$ core of complexes **5a** is best described in terms of having a $\{Mn^{III}(NO^-)\}^6$ core.[9]

Synthesis of Complexes $[Mn(S,S\text{-}C_6H_3\text{-}R)_3]^{2-}$ [R = H (6a), CH_3 (6b)]. The oxygen oxidation reaction of complexes **3a** and **3b** in CH_3CN led to the formation of complexes **2a** and **2b** and the known $[Mn(S,S\text{-}C_6H_3\text{-}R)_3]^{2-}$ [R = H (**6a**), Me (**6b**)] characterized by UV−vis and single-crystal X-ray diffraction (Scheme 2g and 2b′).[17] The ^1H NMR spectrum of complex **6b** at 298 K exhibits the paramagnetic chemical shifts that appear at δ −23.15 (br), −20.33 (br), 18.36 (br), 20.04 (br) ($S,S\text{-}C_6H_3CH_3$) ppm (CD_3CN). The effective magnetic moment of complex **6b** in the solid state, found using the SQUID magnetometer, is from 2.57 μ_B at 2 K to 4.01 μ_B at 299 K (Figure S4 in the Supporting Information). These results support the idea that complex **6a** (or **6b**) adopts a d^3 Mn^{IV} electronic configuration in a distorted octahedral ligand field.

To follow up on our earlier study with a better understanding of the reactivity of the $\{M(NO)\}^n$ (M = transition metal; n = 6,7)-nitrosylated metal thiolates toward oxygen, the reaction of complexes **5a** and **5b** and oxygen was investigated. In contrast to the $\{Fe(NO)\}^6$ complex $[(NO)Fe(S,S\text{-}C_6H_4)_2]^-$ triggering sulfur oxygenation yielding the S-bonded monosulfinate iron nitrosyl species,[15] an attack of oxygen on the $\{Mn(NO)\}^6$ complexes **5a** and **5b** leading to the formation of complexes **4a** and **4b**, the major products $[Mn(S,S\text{-}C_6H_3\text{-}R)_3]^{2-}$ [R = H (**6a**), Me (**6b**)], respectively, identified by IR, UV−vis, and X-ray diffraction and the unidentified byproducts (presumably, the NO-containing byproducts) were observed (Scheme 2e′ and 2h).[18] Many attempts made to isolate and characterize the proposed NO-containing byproducts (nitrite or nitrate) were unsuccessful. Presumably, for the oxygen oxidation of the $\{M(NO)\}^6$ complexes, the electronic structures of the $\{M(NO)\}^6$ centers (M = Fe, Mn) (d^6 Fe^{II} $\{Fe^{II}(NO^+)\}^6$ vs d^4 Mn^{III} $\{Mn^{III}(NO^-)\}^6$) appear to be crucial for the triggering of an inner- or outer-sphere process.[12]

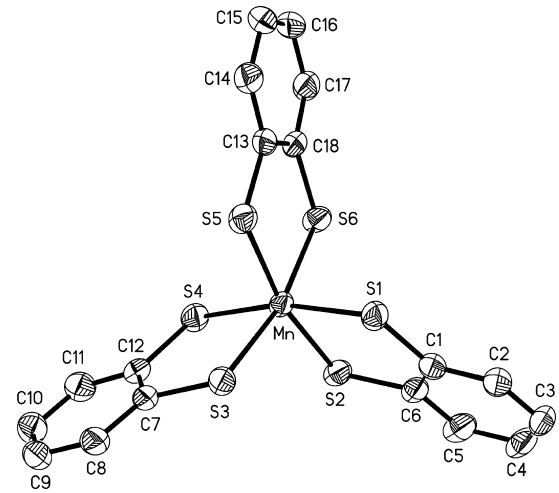

Figure 9. ORTEP drawing of the anionic part ($[Mn(S,S\text{-}C_6H_4)_3]^{2-}$) of complex **6a** with thermal ellipsoids drawn at the 50% probability level. Selected bond distances (Å) and angles (deg): Mn1−S4 2.3430(17), Mn1−S5 2.3220(17), Mn1−S3 2.3355(15), Mn1−S2 2.3248(16), Mn1−S6 2.3270(16), Mn1−S1 2.3309(17); S4−Mn1−S5 103.36(6), S5−Mn1−S3 86.29(6), S2−Mn1−S4 85.37(6), S2−Mn1−S3 102.70(6), S5−Mn1−S6 85.46(6), S2−Mn1−S6 86.78(6), S4−Mn1−S1 167.62(6), S3−Mn1−S1 87.72(6), S6−Mn1−S1 100.59(6).

Structure of Complex 6a. The single-crystal X-ray structure of complex **6a** is depicted in Figure 9, and selected bond coordinates are presented in the figure caption. The geometry of the manganese center is a distorted octahedral. The steric effect among the chelating $[S,S\text{-}C_6H_3R]^{2-}$ ligands from the five-coordinated Mn^{III} complex **2b** to the six-coordinated Mn^{IV} complex **6a** may rationalize an increase of mean Mn−S bond distances of 0.023 Å (Table S1 in the Supporting Information). Obviously, the longer Mn−S bond distances in complex **6a** indicate that the influence of the steric effect of the chelating ligands overwhelms the contraction effect resulting from the oxidation of Mn^{III} (complexes **1a** and **2b**) to Mn^{IV} (complex **6a**).

Conclusion and Comments

The anionic mononuclear $\{Mn(NO)\}^5$ thiolatonitrosylmanganese complex **4a** was obtained from nitrosylation of the

(17) Bressel, U.; Katritzky, A. R.; Lea, J. R. *J. Chem. Soc. A* **1969**, 2258.

(18) (a) Grapperhaus, C. A.; Darensbourg, M. Y. *Acc. Chem. Res.* **1998**, *31*, 451. (b) Kovacs, J. A. *Chem. Rev.* **2004**, *104*, 825. (c) Harrop, T. C.; Mascharak, P. K. *Coord. Chem. Rev.* **2005**, *249*, 3007. (d) Lugo-Mas, P.; Dey, A.; Xu, L.; Davin, S. D.; Benedict, J.; Kaminsky, W.; Hodgson, K. O.; Hedman, B.; Solomon, E. I.; Kovacs, J. A. *J. Am. Chem. Soc.* **2006**, *128*, 11211. (e) Chohant, B. S.; Maroney, M. J. *Inorg. Chem.* **2006**, *45*, 1906.

anionic complex **1a**. Reduction of complex **4a** yielded the dianionic mononuclear $\{Mn(NO)\}^6$ complex **5a**. The coordination environment of $[MnS_4(NO)]$ units and the average Mn−S bond lengths remain intact when complexes **4a** and **4b** were reduced to yield **5a** and **5b**, respectively; however, the observed shortening and lengthening of the Mn−N(O) and N−O bond lengths [1.607(6) and 1.206(8) Å, respectively] for $\{Mn(NO)\}^6$ complex **5a**, compared to the Mn−N(O) and N−O bond lengths of 1.6355(14) and 1.1861(18) Å for $\{Mn(NO)\}^5$ complex **4a**, may rationalize relief of the electron deficiency of the $\{Mn(NO)\}$ core by the electronic change going from $\{Mn(NO)\}^5$ to $\{Mn(NO)\}^6$. X-ray structural data, the IR ν_{NO} spectrum, magnetic measurements, and magnetic fitting results suggest that the electronic structure of complex **4a** is best described as the resonating forms of **A**, **B**, and **C**, with major contributions from **B** and **C** forms, as shown in Scheme 1. Also, IR, UV−vis, and magnetic susceptibility measurements suggest that the electronic structure of the $\{Mn(NO)\}^6$ core of complexes **5a** and **5b** may exist as $\{(L)(L)Mn^{III}(NO^-)\}$, i.e., the $\{Mn(NO)\}^6$ having a high-spin d^4 $Mn^{III}NO^-$ electronic configuration in a distorted square-pyramidal ligand field.[9] In contrast to the $\{Fe(NO)\}^6$ $[(NO)Fe(S,S\text{-}C_6H_4)_2]^-$ initiating sulfur oxygenation of iron thiolate by molecular oxygen to yield S-bonded monosulfinate iron complex $[(NO)Fe(SO_2,S\text{-}C_6H_4)(S,S\text{-}C_6H_4)]^-$,[15] oxygen oxidation of the $\{Mn(NO)\}^6$ complex **5a** led to the formation of complex **4a** and the major product **6a** identified by IR, UV−vis, and X-ray diffraction. Presumably, factors contributing to the distinct oxidation pathways are attributed to the different electronic structures of the $\{M(NO)\}^6$ core (M = Fe, Mn) between $\{Fe(NO)\}^6$ complex $[(NO)Fe(S,S\text{-}C_6H_4)_2]^-$ (d^6 Fe^{II} $\{Fe^{II}(NO^+)\}^6$) and $\{Mn(NO)\}^6$ complexes **5a** and **5b** (d^4 Mn^{III} $\{Mn^{III}(NO^-)\}^6$, the weaker $M_{d\pi}-S_{p\pi}$ interaction).[18]

Experimental Section

Manipulations, reactions, and transfers of samples were conducted under nitrogen according to standard Schlenk techniques or in a glovebox (nitrogen gas). Solvents were distilled under nitrogen from appropriate drying agents [diethyl ether from CaH_2, acetonitrile from $CaH_2-P_2O_5$, methylene chloride from P_2O_5, hexane and tetrahydrofuran (THF) from sodium benzophenone] and stored in dried, nitrogen-filled flasks over 4 Å molecular sieves. Nitrogen was purged through these solvents before use. The solvent was transferred to a reaction vessel via a stainless steel cannula under positive pressure of nitrogen. The reagents 1,2-benzenedithiol, toluene-3,4-dithiol, sodium methoxide, bis(triphenylphosphine)iminium chloride, manganese(II) bromide, tetraethylammonium chloride, and bis(triphenylphosphine)iminium borohydride (Lancaster/Acros/Aldrich/Fluka) were used as received. IR spectra of the π_{NO} stretching frequencies were recorded on a Perkin-Elmer model Spectrum One B spectrophotometer with sealed solution cells (0.1 mm) and KBr windows. UV−vis spectra were recorded on GBC Cintra 10e and Hewlett-Packard 71 spectrophotometers. Analyses of carbon, hydrogen, and nitrogen were obtained with a CHN analyzer (Heraeus).

Preparation of [cation][(THF)Mn(L)$_2$] [THF = tetrahydrofuran, L = 1,2-benzenedithiolate, cation = PPN$^+$ (1a); toluene-3,4-dithiolate, cation = Et$_4$N$^+$ (1b)]. A MeOH solution (7 mL) of [Na][OMe] (4 mmol, 0.216 g) was added slowly to toluene-3,4-dithiol (2 mmol, 246 μL) or 1,2-benzenedithiol (2 mmol, 260 μL). After the reaction solution was stirred for 20 min, the mixture solution was added to a THF solution (5 mL) of $MnBr_2$ (1 mmol, 0.215 g) via cannula under nitrogen. After the reaction solution was stirred for another 2 h at ambient temperature, the red-brown mixture solution was then transferred to another Schlenk flask containing $[Et_4N][Br]$ (2 mmol, 0.420 g) or [PPN][Cl] (2 mmol, 1.148 g). The reaction solution was then stirred overnight, and the mixture solution was filtered through Celite to remove NaBr (NaCl) and the insoluble solid. Diethyl ether was then added into the filtrate to precipitate the reddish-brown solid [cation][(THF)Mn(L)$_2$] [THF = tetrahydrofuran, L = 1,2-benzenedithiolate, cation = PPN$^+$ (**1a**); toluene-3,4-dithiolate, cation = Et$_4$N$^+$ (**1b**)] (yield 61% for **1a** and 55% for **1b**). Diffusion of diethyl ether into a THF solution of complex **1a** at −15 °C for 3 days yielded reddish-brown crystals suitable for X-ray crystallography. Complex **1a**. ^{1}H NMR (C_4D_8O): δ 3.62 (s), 1.78 (s) (C_4H_8O), −8.16 (br), −22.95 (br) (S,S-C_6H_4) ppm. Absorption spectrum (THF) [λ_{max}, nm (ϵ, M^{-1} cm^{-1})]: 352 (14 837), 540 (748). Anal. Calcd for $C_{52}H_{46}MnNOP_2S_4$: C, 66.00; H, 4.86; N, 1.45. Found: C, 66.02; H, 4.75; N, 1.49. Complex **1b**. Absorption spectrum (THF) [λ_{max}, nm (ϵ, M^{-1} cm^{-1})]: 355 (19 215), 552 (986).

Preparation of [cation]$_2$[Mn(L)$_2$]$_2$ [L = 1,2-benzenedithiolate, cation = PPN$^+$ (2a); toluene-3,4-dithiolate, cation = Et$_4$N$^+$ (2b)]. Complex **1a** (0.4 mmol, 0.378 g) or complex **1b** (0.4 mmol, 0.224 g) was loaded into a 20-mL Schlenk tube, and then 15 mL of the degassed CH_2Cl_2 was added via cannula under positive nitrogen. CH_2Cl_2 solutions of complexes **1a** and **1b** were stirred for 10 min at ambient temperature, and then the solution was filtered through Celite to remove the insoluble solid. Diethyl ether was added to precipitate the red-brown solid [PPN]$_2$[Mn(L)$_2$]$_2$ [L = 1,2-benzenedithiolate (**2a**); toluene-3,4-dithiolate, cation = Et$_4$N$^+$ (**2b**)] (yield 80% for **2a** and 78% for **2b**). Diffusion of diethyl ether into CH_2Cl_2 solutions of complexes **2a** and **2b** at −15 °C yielded red-brown crystals suitable for single-crystal X-ray diffraction. Complex **2a**. ^{1}H NMR (CD_2Cl_2): δ −24.57 (br), −4.17 (br) (S,S-C_6H_4) ppm. Absorption spectrum (CH_2Cl_2) [λ_{max}, nm (ϵ, M^{-1} cm^{-1})]: 538 (1458), 639 (426), 895 (193). Anal. Calcd for $C_{96}H_{76}Mn_2N_2P_4S_8$: C, 65.96; H, 4.38; N, 1.6. Found: C, 65.82; H, 4.30; N, 1.41. Complex **2b**. Absorption spectrum (CH_2Cl_2) [λ_{max}, nm (ϵ, $M^{-1}cm^{-1}$)]: 538 (2952), 639 (196), 895 (90).

Preparation of [cation]$_2$[Mn(L)$_2$] [L = 1,2-benzenedithiolate, cation = PPN$^+$ (3a); toluene-3,4-dithiolate, cation = Et$_4$N$^+$ (3b)]. Complex **2a** (0.4 mmol, 0.564 g) or complex **2b** (0.4 mmol, 0.394 g) was loaded into a 20-mL Schlenk tube, and the degassed CH_3CN (9 mL) was added via cannula under positive nitrogen. The CH_3CN solution of complex **2a** was then transferred slowly into another Schlenk flask containing $[PPN][BH_4]$ (1 mmol, 0.553 g) or $[Et_4N][BH_4]$ (1 mmol, 0.145 g) via cannula under positive nitrogen. The resulting mixture was stirred for 5 min at room temperature, and then the light-yellow mixture solution was filtered through Celite to remove the insoluble solid. Degassed diethyl ether was added into the filtrate to precipitate the light-yellow solid [PPN]$_2$[Mn(L)$_2$] (**3a**; L = 1,2-benzenedithiolate) (yield 37%).[15] Diffusion of diethyl ether into a CH_3CN solution of complex **3a** at room temperature yielded light-yellow crystals suitable for X-ray crystallography. Complex **3a**. Absorption spectrum (CH_3CN) [λ_{max}, nm (ϵ, M^{-1} cm^{-1})]: 521 (444), 370 (8895). Anal. Calcd for $C_{84}H_{68}MnN_2P_4S_4$: C, 71.42; H, 4.85; N, 1.98. Found: C, 70.82; H, 4.89; N, 2.08. Complex **3b**. Absorption spectrum (CH_3CN) [λ_{max}, nm (ϵ, M^{-1} cm^{-1})]: 521 (865), 370 (8355).

Preparation of [cation][(NO)Mn(L)$_2$] [L = 1,2-benzenedithiolate, cation = PPN$^+$ (4a); toluene-3,4-dithiolate, cation = Et$_4$N$^+$ (4b)]. The THF solution (15 mL) of complex **1a** (0.4 mmol, 0.378 g) was purged by NO(g) (10% NO + 90% N_2) for 5 min at 0 °C,

and then the solution was stirred for 10 min at 0 °C. Degassed diethyl ether was then added to precipitate the deep-brown solid [PPN][(NO)Mn(L)$_2$] (**4a**; L = 1,2-benzenedithiolate) (yield 91%). Diffusion of diethyl ether into a THF solution of complex **4a** at −15 °C yielded deep-brown crystals suitable for X-ray crystallography. Complex **4a**. IR ν_{NO}: 1735 s cm^{-1} (THF), 1729 s cm^{-1} (KBr). Absorption spectrum (CH_2Cl_2) [λ_{max}, nm (ϵ, M^{-1} cm^{-1})]: 727 (1369). Anal. Calcd for $C_{48}H_{38}MnN_2OP_2S_4$: C, 63.78; H, 4.24; N, 3.10. Found: C, 63.07; H, 4.71; N, 2.48. Complex **4b**. IR ν_{NO}: 1735 s cm^{-1} (THF), 1727 s cm^{-1} (KBr). Absorption spectrum (CH_2Cl_2) [λ_{max}, nm (ϵ, M^{-1} cm^{-1})]: 740 (1483).

Preparation of [cation]$_2$[(NO)Mn(L)$_2$] [L = 1,2-benzenedithiolate, cation = PPN$^+$ (5a); toluene-3,4-dithiolate, cation = Et$_4$N$^+$ (5b)]. NO(g) (10% NO + 90% N_2) was purged through the CH_3CN−MeOH (light-yellow) solutions of complexes **3a** and **3b**, freshly prepared from the addition of CH_3CN solutions (9 mL) of complexes **2a** and **2b** (0.5 mmol) into a MeOH solution (3 mL) of [PPN][BH_4] (1 mmol, 0.553 g) or [Et_4N][BH_4] (1 mmol, 0.145 g) and stirred for 5 min at ambient temperature. A significant change in color of the reaction solution from light-yellow to deep-green was observed. The solution was filtered through Celite to remove the insoluble solid. Diethyl ether (25 mL) was added to precipitate the deep-green solid [cation]$_2$[(NO)Mn(L)$_2$] [L = 1,2-benzenedithiolate, cation = PPN$^+$ (**5a**); toluene-3,4-dithiolate, cation = Et$_4$N$^+$ (**5b**)] (yield 85% for **5a** and 78% for **5b**). Diffusion of diethyl ether into CH_3CN solutions of complexes **5a** and **5b** at room temperature yielded deep-green crystals suitable for X-ray crystallography. Complex **5b**. IR ν_{NO}: 1648 s cm^{-1} (CH_3CN), 1651 s cm^{-1} (KBr). Absorption spectrum (CH_3CN) [λ_{max}, nm (ϵ, M^{-1} cm^{-1})]: 362 (6621), 667 (1569). Anal. Calcd for $C_{30}H_{52}N_3OS_4Mn$: C, 55.13; H, 7.96; N, 6.43. Found: C, 54.69; H, 8.32; N, 6.09. Complex **5a**. IR ν_{NO}: 1651 s cm^{-1} (CH_3CN), 1651 s cm^{-1} (KBr). Absorption spectrum (CH_3CN) [λ_{max}, nm (ϵ, M^{-1} cm^{-1})]: 357 (6581), 665 (2274). Alternatively, complex **4a** (0.4 mmol, 0.362 g) or complex **4b** (0.4 mmol, 0.210 g) was loaded into a 20-mL Schlenk tube, and the degassed CH_3CN (9 mL) was added via cannula under positive nitrogen. The CH_3CN solution of complexes **4a** and **4b** were then transferred slowly into another Schlenk flask containing a CH_3CN solution (3 mL) of [PPN][S,NH_2-C_6H_4] (0.4 mmol, 0.265 g) via cannula under positive nitrogen. The resulting mixture solution was stirred for 2 h at room temperature, and the color of the solution changed from deep-brown to deep-green. Diethyl ether (25 mL) was then added to precipitate the deep-green solid **5a** and **5b**. The solution was then separated from the deep-green solid and dried under vacuum to give 2-aminophenyl disulfide identified by ^{1}H NMR.

Preparation of Complex [cation]$_2$[Mn(L)$_3$] [L = 1,2-benzenedithiolate, cation = PPN$^+$ (6a); toluene-3,4-dithiolate, cation = Et$_4$N$^+$ (6b)]. Pure oxygen gas (10 mL) was injected into CH_3CN solutions of complexes **5a** and **5b** (0.4 mmol), and then the reaction solution was stirred for 30 min at room temperature. A significant change in the color of the reaction solution from deep-green to dark-green was observed, and then the solution was filtered through Celite to remove the insoluble solid. Degassed diethyl ether (25 mL) was added to precipitate the dark-green solid. The filtrate (red-brown solution) was dried under vacuum and redissolved in THF. Hexane was then added to precipitate the red-brown solid identified by IR and UV−vis as complexes **4a** and **4b**. The dark-green solid was characterized by UV−vis as complexes [cation]$_2$[Mn(L)$_3$] [L = 1,2-benzenedithiolate, cation = PPN$^+$ (**6a**); toluene-3,4-dithiolate, cation = Et$_4$N$^+$ (**6b**)]. Complex **6b**. ^{1}H NMR (CD_3CN): δ 20.04 (br), 18.36 (br), −20.33 (br), −23.15 (br) (S,S-$C_6H_4CH_3$) ppm. Absorption spectrum (CH_3CN) [λ_{max}, nm (ϵ, M^{-1} cm^{-1})]: 363 (8436), 508 (1916), 582 (1488), 741 (1265). Anal. Calcd for $C_{37}H_{58}N_2S_6Mn$: C, 57.14; H, 7.46; N, 3.60. Found: C, 57.26; H, 7.88; N, 3.15. Complex **6a**. Absorption spectrum (CH_3CN) [λ_{max}, nm (ϵ, M^{-1} cm^{-1})]: 363 (8530), 502 (1328), 575 (1032), 727 (736). Diffusion of diethyl ether into a CH_3CN solution of complex **6a** at room temperature yielded dark-green crystals suitable for X-ray crystallography.

Magnetic Measurements. The magnetic data were recorded on a SQUID magnetometer (MPMS5 Quantum Design Co.) under a 0.5 T external magnetic field in the temperature range of 2−300 K for complexes **1a**, **2a**, **2b**, **4a**, and **5a** (2−299 K for complex **6b**). The magnetic susceptibility data were corrected with TIP (2×10^{-4} cm^3 mol^{-1}) and ligands' diamagnetism by the tabulated Pascal's constants.[19]

Crystallography. Crystallographic data of complexes **1a**, **2b**, **3a**, **4a**, **5a**, and **6a** are summarized in the Supporting Information. The crystals of **1a**, **2b**, **3a**, **4a**, **5a**, and **6a** are chunky. Each crystal was mounted on a glass fiber. Diffraction measurements for complexes **2b** and **4a** were carried out at 100(2) K on a CCD area detector [150(2) K for complexes **5a** and **6a** on a Nonius Kappa CCD, 293(2) K for **1a** on a CAD4 diffractometer (point detector), and 150(2) K for complex **3a**] on a Bruker SMART Apex CCD diffractometer with graphite-monochromated Mo Kα radiation (λ 0.7107 Å) and θ between 1.63 and 25.00° for complex **1a**, between 1.47 and 28.36° for complex **2b**, between 1.66 and 27.50° for complex **3a**, between 1.27 and 28.31° for complex **4a**, between 2.18 and 27.50° for complex **5a**, and between 1.56 and 27.50° for complex **6a**. In the case of complex **5a**, Mn and NO were found at disordered positions (shown in the crystallographic data), and only one of the disordered positions is shown in Figure 8. Least-squares refinement of the positional and anisotropic thermal parameters for the contribution of all non-hydrogen and hydrogen atoms was fixed at calculated positions and refined as riding models. An absorption corrections were made for **1a** (PSI-SCAN), **2b** (Empirical), **3a** (*SADABS*[20]), **4a** (Empirical), and **5a** and **6a** (*SORTAV*[21]). The *SHELXTL*[22] structure refinement program was employed.

Acknowledgment. We gratefully acknowledge financial support from the National Science Council of Taiwan and facilities from the National Center for High-performance Computing.

Supporting Information Available: X-ray crystallographic files in CIF format for the structure determinations of [PPN][(THF)Mn(S,S-C_6H_4)$_2$], [Et_4N]$_2$[Mn(S,S-$C_6H_3CH_3$)$_2$]$_2$, [PPN]$_2$[Mn(S,S-C_6H_4)$_2$], [PPN][(NO)Mn(S,S-C_6H_4)$_2$], [PPN]$_2$[(NO)Mn(S,S-C_6H_4)$_2$], and [PPN]$_2$[Mn(S,S-C_6H_4)$_3$], plots of the effective magnetic moment (μ_B) versus temperature for complexes **1a**, **2a**, **2b**, and **6b**, and tables of bond lengths and angles and of crystal data and structure refinement. This material is available free of charge via the Internet at http://pubs.acs.org.

IC801553S

(19) (a) O'Connor, C. J. *Prog. Inorg. Chem.* **1982**, *29*, 203. (b) Bain, G. A.; Berry, J. F. *J. Chem. Educ.* **2008**, *85*, 532–536.
(20) Sheldrick, G. M. *SADABS, Siemens Area Detector Absorption Correction Program*; University of Göttingen: Göttingen, Germany, 1996.
(21) SORTAV: Blessing, R. H. *Acta Crystallogr., Sect A: Fundam. Crystallogr.* **1995**, *51*, 33.
(22) Sheldrick, G. M. *SHELXTL, Program for Crystal Structure Determination*; Siemens Analytical X-ray Instruments Inc.: Madison, WI, 1994.